Proceedings of
ASME TURBOEXPO 2000
May 8-11, 2000, Munich Germany

2000-GT-433

INVESTIGATION OF THE FLOWFIELD IN THE TRANSONIC VKI BRITE EURAM TURBINE STAGE WITH 3D STEADY AND UNSTEADY N-S COMPUTATIONS

Björn Laumert*, **Hans Mårtensson**
Volvo Aero Corporation
Propulsion Systems
Military Engines Division
461 81 Trollhättan, Sweden

Torsten H. Fransson
KTH - Royal Institute of Technology
Div. of Heat and Power Technology
100 44 Stockholm, Sweden

ABSTRACT

This paper presents the results from three-dimensional (3D) steady and unsteady Navier-Stokes computations, performed on the transonic VKI BRITE EURAM test turbine stage. The work aimed at giving deeper insight in the aerodynamics of the turbine stage. The analysis has been carried out with the nominal stator trailing edge ejection slot geometry and cooling flow ejection. Additionally a simplified rounded stator trailing edge was employed. The results from the unsteady computations were compared with measured pressure perturbation traces at 22 locations around the rotor blade at midspan. Computations with both the ejection slot and the rounded stator trailing edge geometry were in good agreement with the measurements on the pressure side and half chord of the rotor blade's suction side. Measurements and computations showed less good agreement downstream a weak shock on the suction side of the rotor blade. The measured pressure double peak in the rotor blade leading edge region is only observed in the computations with the ejection slot geometry.

INTRODUCTION

Much research effort has been dedicated to understand and describe the aerodynamics in turbine stages. Three-dimensional effects like secondary passage vortices and tip leakage vortex as well as unsteady effects due to rotor-stator interaction feature the complex flow field in turbine stages. It is commonly acknowledged that these features have an impact on the heat transfer and mechanical loading of the turbine rotor and therefore play an important role for blade failure governed by heat strain and high cycle fatigue. In high-pressure transonic turbines stages the deterministic unsteadiness experienced by the rotor blade row originates predominantly from three different sources (Doorly and Oldfield 1985). Firstly, fluctuations arising from the interaction between the potential fields of adjacent blade rows propagate both upstream and downstream. Secondly, the upstream stator wake is continuously "chopped" and distorted by the rotor blades and convected downstream through the rotor blade passage. Thirdly, the rotor interferes with stator trailing edge shocks giving rise to complex unsteady shock patterns in the inter blade row region (Giles 1988, Saxer and Giles 1994).

Recent experimental research on rotating turbine facilities has provided useful data for the development and validation of unsteady CFD codes. With today's computer resources the CFD solvers are now considered useful as design tools for turbine applications. Furthermore, they also enable us to gain a better insight into complex unsteady flow phenomena. The results from computations with 2D Navier Stokes solvers have shown good agreement with measurements regarding the unsteady pressure field around the stator and rotor blades in transonic turbines at mid span, where the influence of 3D effects is rather weak (Hilditch et al 1998). In regions with strong influence of 3D effects near the hub and shroud these solvers proved to be less useful (Moss et al 1997). These results suggest that the employment of a fully 3D unsteady flow solver is necessary when the aim is to predict the entire flow field in a turbine stage.

* presently graduate student at the Royal Institute of Technology

Copyright © 2000 by ASME
Downloaded From: http://proceedings.asmedigitalcollection.asme.org/ on 02/03/2016 Terms of Use: http://www.asme.org/about-asme/terms-of-use

The objective of the work presented in this paper is to gain deeper insight into the unsteady flow phenomena that arise in the VKI BRITE EURAM transonic turbine stage, guided by the results from 3D steady and unsteady computations performed with the Navier Stokes solver VOLSOL. The reliability of the simulation method was investigated by comparing the computational results with measurement data reported by Denos et al (1999). In computational investigations of turbine aerodynamics, blade trailing edge ejection slots are often approximated with rounded trailing edges. An investigation of the influence of this simplification on the computed steady and unsteady flow field of the test turbine stage was also conducted.

NOMENCLATURE

a	speed of sound
c_{sax}	stator axial chord
ES	ejection slots
$\dot{m}$	mass flow
P	static pressure
P_0	total pressure
STE	stator trailing edge
T	static temperature
T_0	total temperature
V	velocity
β	rotor relative inlet angle
φ	phase, defining the position of the rotor blade

subscripts

ax	axial
s	stator
w	wall
1	stator inlet condition
2	stator outlet, rotor inlet
3	rotor outlet

TEST CASES AND BOUNDARY CONDITIONS

The computations were performed on the VKI BRITE EURAM test turbine geometry. A large experimental program (Denos et al 1999), which covered the investigation on effects of variations in rotor speed, axial stator–rotor gap and stator trailing edge cooling flow ejection, was carried out on the transonic turbine stage and the results served as reference data in the computations.

The computed test cases are summarized in Table 1 together with mass averaged mass flow, rotor relative inlet angle and static pressure, computed at $0.23c_{sax}$ behind the stator trailing edge. For the computations the nominal rotor speed of 6500 RPM together with an axial stator–rotor gap of 35% axial stator chord was chosen as the base configuration. At 6500 RPM the measurements showed that the test conditions were very close to the design conditions.

Base conditions: P_{01}= 1.6278 bar at midspan T_{01}= 441.6 K at midspan P_3= 0.5325 bar at hub T_w= 293 K Rotor speed =6500 rpm Number of blades= 42/63 Turbulence model: k-ε standard wall functions			
STE geometry/comp.	$\dot{m}$ [kg/s]	β [deg]	P_2 [bar]
Rounded/steady	10.33	43.1	0.839
Rounded/unsteady	10.28	42.9	0.839
ES 0% /steady	10.53	41.3	0.861
ES 3% /steady	10.64	40.5	0.865
ES 3% /unsteady	10.62	41	0.868
Changed parameter: Rotor speed = 6000 rpm. Others as base conditions.			
Rounded/steady	10.32	48.2	0.826
Changed parameter: Number of blades=43/64. Others as base conditions.			
Rounded/steady	10.22	43.8	0.832
ES 0% /steady	10.41	42	0.854
Changed parameter: T_{01}= 420 K at midspan. Others as base conditions.			
Rounded/steady	10.56	41.1	0.845
Changed parameter: T_{01}= 460 K at midspan. Others as base conditions.			
Rounded/steady	10.1	44.7	0.836
Changed parameter Turbulence model: k-ε Low Reynolds. Others as base cond.			
Rounded/steady	10.36	42.6	0.844

TABLE 1: COMPUTED CASES WITH PREDICTED MASS FLOW, RELATIVE ROTOR INLET ANGLE AND STATIC PRESSURE AT $0.23c_{sax}$ BEHIND THE STATOR TRAILING EDGE.

The operating conditions were used as boundary conditions for the computations. Pressure-based boundaries were specified at stage inlet and outlet. Inlet conditions were given as radial profiles of total pressure and temperature. At the stage outlet a radial pressure equilibrium condition was imposed. Temperature walls were employed with a non-slip boundary condition.

Computations were performed with different rotor velocities to determine the influence of a rotor inlet angle change on the pressure distribution on the rotor blade. The inlet total temperature was changed in order to simulate the influence of the experimental test to test variations on the pressure predictions. Steady computations with resolved boundary layers instead of wall functions were performed to investigate the influence of the boundary layer treatment on the solution.

In the experimental investigations a stator vane geometry with a trailing edge ejection slot cut out was utilized. Two different stator trailing edge geometries were used for the

Copyright © 2000 by ASME
Downloaded From: http://proceedings.asmedigitalcollection.asme.org/ on 02/03/2016 Terms of Use: http://www.asme.org/about-asme/terms-of-use

computations. In addition to the stator trailing edge geometry with the ejection slot cut out, a simplified stator blade with a rounded trailing edge was employed. A cooling flow injection of 3% of the stage mass flow was simulated with the ejection slot configuration.

The test stage consists of 43 stator and 64 rotor blades. In order to facilitate the periodicity requirement, the number of blades were reduced to 42 and 63, respectively. Two stator and three rotor passages were used for the unsteady sliding grid computations. Steady mixing plane computations were performed with both the reduced number of blades and the real geometry. A comparison of the steady computations performed with the real and reduced number of blades showed a difference of 0.7 degrees in relative rotor inlet angle and a difference of 1.2% in stage mass flow (see also Table 1). As shown in Fig.1 the predicted pressure around the rotor blade at midspan differs less then 1% between the computations with the real and the reduced number of blades. The differences were considered to be relatively small and therefore the blading was not scaled for the configuration with the reduced number of blades.

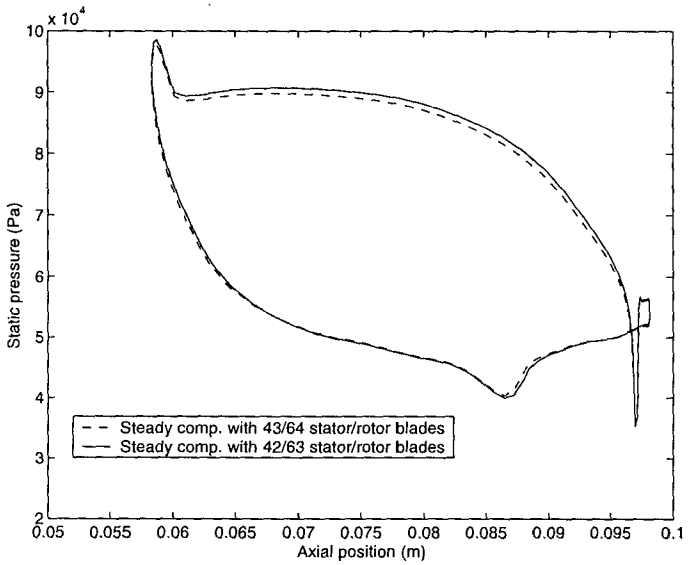

FIG. 1: COMPUTED STATIC PRESSURE DISTRIBUTION AROUND THE ROTOR BLADE AT MIDSPAN. REAL AND REDUCED NUMBER OF BLADES.

FLOW SOLVER DESCRIPTION

NUMERICAL METHOD

The equations used to model the flow are the Favre–averaged Navier Stokes equations for compressible flow expressed in the cartesian coordinate system. The equations are extended to turbulent flow using the k–ε turbulence model formulation with standard wall functions and Chien's Low Reynolds model.

The 3D Navier Stokes flow solver VOLSOL developed at Volvo Aero Corporation was used. The numerical method to solve the governing equations is based on an explicit, time–marching, cell–centered finite-volume procedure. The convective fluxes are reconstructed with a third order upwind biased scheme, which is based on the characteristic variables and associated characteristic velocities. The viscous fluxes are computed with a compact second order accurate centered flux scheme. Time integration is handled with an explicit three–stage Runge–Kutta procedure. Local time step acceleration is used for steady state solutions. Eriksson (1990) provided a detailed description of the numerical method.

STATOR–ROTOR INTERFACE

Two approaches were used to pass flow information between the stator and the rotor frame of reference:

- For the steady computations a mixing plane method was employed. The conservative variables are averaged in tangential direction for all constant radius cell face rows at the interface in the stator and rotor frame of reference and associated characteristic variables are computed. These are used as absorbing boundary conditions. Initial fluxes are calculated from both sides of the interface. Final fluxes are calculated by tangentially integrating these initial fluxes on both sides and distributing appropriate flux corrections in order to obtain exact conservation of mass, momentum and energy.
- For the unsteady computations a sliding grid method was employed.

Both methods are second order accurate. A condition for flux conservation at the interface is that the grid has the same radial node distribution on each side of the interface.

GAS INJECTION MODEL

An integral film cooling injection model simulates gas injection by adding the influence of the penetrating jets as source terms in the governing equation. The injection region, mass flow, Mach number and temperature of the injected gas are specified as user input based on empirical basis or experience. Details of the method have been presented by Dahlander et al (1998).

GRIDS AND BOUNDARY LAYER TREATMENT

The flow solver uses structured multi-block grids built with Volvo's in-house code G3DMESH. This grid generation code uses a parameter-controlled module-script, designed for turbine blades. The grids are non-orthogonal body-fitted.

Mixing plane computations were performed on a single blade-passage grid. An O-grid was used around the blades with controlled stretching in the direction normal to the wall. The boundary layers were resolved down to a y+ mean value of 28 for standard wall function computations. Additionally Low Reynolds computations were conducted with a y+ mean value of 1.2. The computational grid at midspan for mixing plane

Copyright © 2000 by ASME
Downloaded From: http://proceedings.asmedigitalcollection.asme.org/ on 02/03/2016 Terms of Use: http://www.asme.org/about-asme/terms-of-use

standard wall functions computations is shown in Fig. 2. Unsteady computations were performed with the standard wall functions grid described above with two stator and three rotor passages. Table 2 lists the grid sizes for all test cases.

The stator trailing edge ejection slots were implemented into the standard wall functions grid with the rounded edge geometry by adding an extra grid block. Fig. 3 shows the grid in the stator trailing edge region at midspan for both geometries.

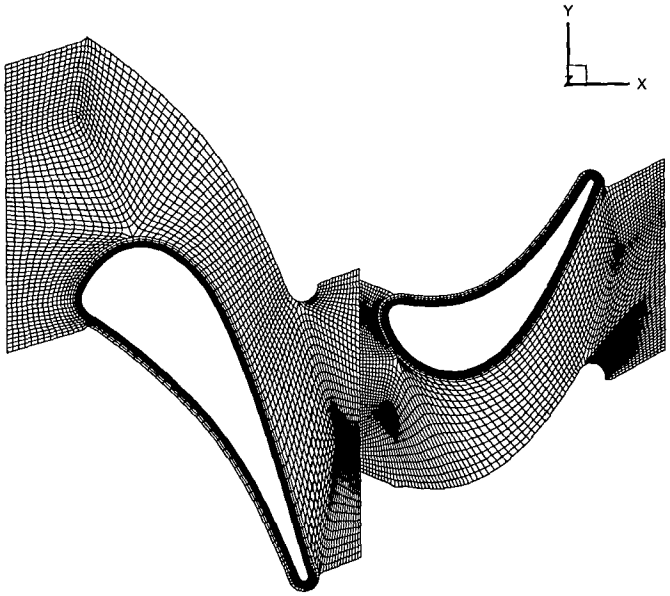

FIG. 2: GRID AT MIDSPAN USED FOR MIXING PLANE COMPUTATIONS.

Computation method	Total number of nodes	Nodes in radial direction
Steady/standard wall fun.	303125	36
Steady/Low Reynolds	870520	70
Unsteady/standard wall fun.	759039	36

TABLE 2: TEST CASE GRID SIZES.

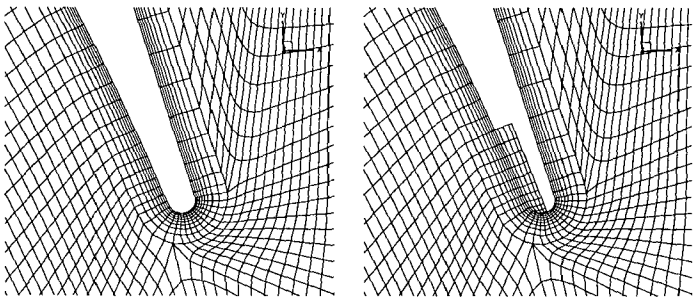

FIG. 3: GRID AT STATOR TRAILING EDGE WITH ROUNDED EDGE AND EJECTION SLOT GEOMETRY.

COMPUTATIONAL APPROACH

The PVM software package was used for code parallelization. Steady computations were performed on two processors and unsteady computations on eight processors on a HP V-class machine. The steady state solutions needed 15000 time steps for convergence. They were used as initial conditions for the unsteady computations, which needed 4400 time steps per period. The size of the maximum deviation in static pressure on the rotor blade at midspan between two periods served as convergence criteria. Convergence was reached after eight periods, when the deviation was less then 0.1%. Due to the nonlinear processes convergence to exactly zero in this sense cannot be expected, as sub harmonics and/or portions of uncoherent flow may be present.

RESULTS AND DISCUSSION

The results presented below were obtained with fully 3D steady and unsteady computations. As earlier shown in Fig. 1, the change of the nominal number of blades from 43/64 to 42/63 was proven to have only small influence on the predicted pressure on the rotor blade surface for the steady computations. Beside this change in the stage geometry no other simplifications were introduced. Both the stator trailing edge cut out and the rotor tip clearance were implemented in the computational grid. Additionally, computations were performed with a simplified geometry, which proved to have a considerable influence on the solution for both steady and unsteady computations.

The three dimensionality of the flow is visualized in Fig. 4 and 5 with computed radial velocity contour plots along the stator and rotor suction side. The regions near the hub and shroud with large radial velocities indicate the presence of typical secondary flow vortices. It can be seen that endwall vortices are present in both the stator and rotor passage. At the top of the rotor suction side the tip leakage vortex is visible. These flow features have influence on the global flow field and their presence is therefore a precondition for a complete flow field description.

The investigation was concentrated on the prediction of the static pressure distribution around the rotor blade at midspan. The predicted steady static pressure distribution on the rotor blade surface at midspan is in line with the results from other computations independently performed by Michelassi et al. (1998) and by Denos et al. (1999). All computations report a significantly higher static pressure on the front suction side of the blade compared with the measurements performed by Denos et al. (1999). Fig. 6 shows the pressure distribution around the rotor blade computed with VOLSOL, compared with the computations by Denos et al. (1999) and measurements. The discrepancy between computations and measurements can be explained with a difference in rotor incidence. Despite an extensive investigation considering measurement uncertainties, leakage flow, flow separation, unsteady effects and turbulence model, the difference in rotor incidence between computations and measurements remains unexplained.

Copyright © 2000 by ASME
Downloaded From: http://proceedings.asmedigitalcollection.asme.org/ on 02/03/2016 Terms of Use: http://www.asme.org/about-asme/terms-of-use

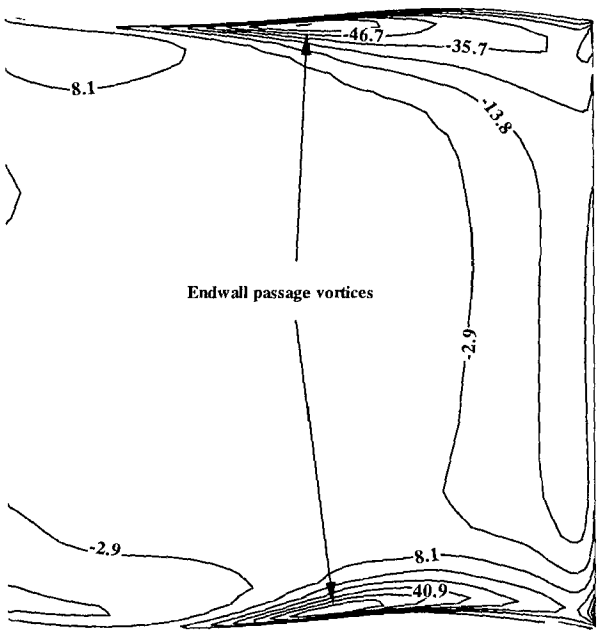

FIG. 4: RADIAL VELOCITY CONTOURS AT THE STATOR SUCTION SIDE FOR WALL FUNCTIONS COMPUTATIONS. THE VELOCITY IS VISUALIZED AT THE FIRST COMPUTATIONAL NODE IN THE FLOW DOMAIN.

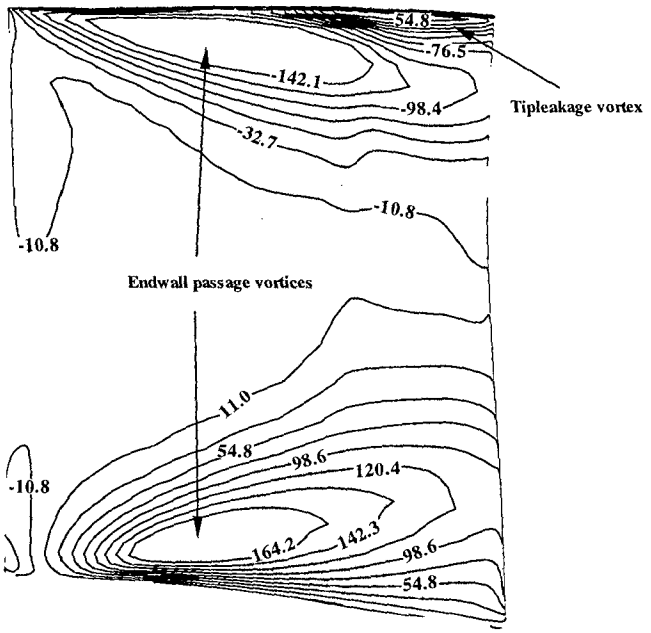

FIG. 5: RADIAL VELOCITY CONTOURS AT THE ROTOR SUCTION SIDE FOR WALL FUNCTIONS COMPUTATIONS. THE VELOCITY IS VISUALIZED AT THE FIRST COMPUTATIONAL NODE IN THE FLOW DOMAIN.

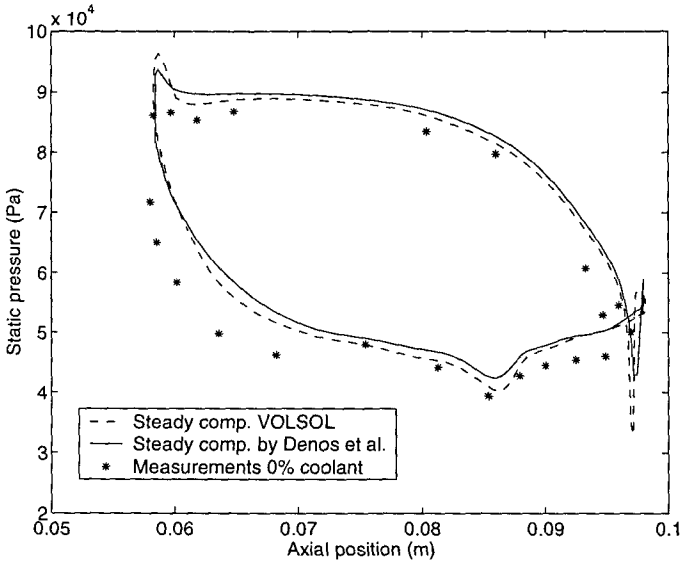

FIG. 6: STATIC PRESSURE DISTRIBUTION AROUND THE ROTOR BLADE AT MIDSPAN. COMPUTATIONS AND MEASUREMENTS.

Though the unsteady computations show no improvement compared with the measurements regarding the time averaged static pressure on the rotor blade surface, the computed unsteady pressure perturbations at the same location are both in phase and amplitude in good agreement with the measurements.

STEADY COMPUTATIONS

Steady mixing plane computations were performed with the rounded stator trailing edge and the ejection slot geometry. The latter configuration was computed with 0% and 3% coolant ejection. The resulting static pressure distribution around the rotor blade at midspan is presented in Fig. 7 together with time averaged measurements with 0% and 3% cooling flow ejection.

The prediction is poor on the front suction side of the rotor blade where all configurations over estimate the static pressure. Computations and measurements merge together again at the crown of the blade. The predicted location of a weak shock at the rear suction side, indicated by the bump in the static pressure, is in good agreement with the measurements. A computation performed with a rotor velocity of 6000 rpm showed good agreement with the measurements. The computations would suggest a difference in relative rotor inlet angle of 5.1 degrees. See also Table 1. These observations are in agreement with the results from Denos et al. (1999). The results described above were performed with standard wall functions. Steady computations with resolved boundary layers and the low Reynolds model on the rounded edge geometry showed no improvement. There is no obvious explanation for an error in rotor incidence. Neither the oil flow visualization and loss measurements on the stator annular cascade performed by Sieverding et al. (1996) nor the computations did reveal any flow separation on the stator blade which could have led to a stator exit angle deviation.

Copyright © 2000 by ASME
Downloaded From: http://proceedings.asmedigitalcollection.asme.org/ on 02/03/2016 Terms of Use: http://www.asme.org/about-asme/terms-of-use

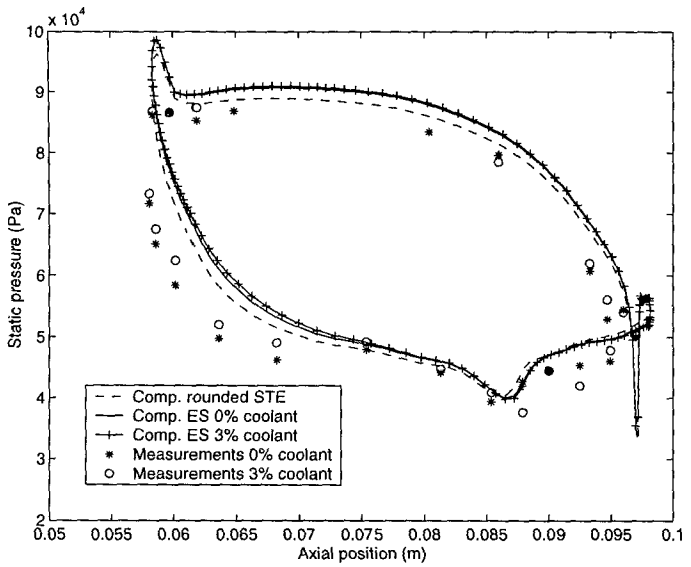

FIG. 7: STATIC PRESSURE DISTRIBUTION AROUND THE ROTOR BLADE AT MIDSPAN. COMPUTATIONS AND MEASUREMENTS.

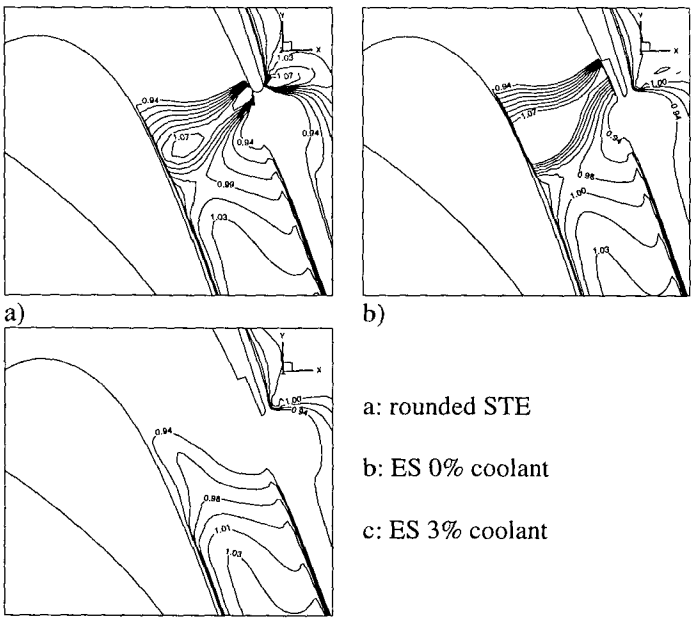

FIG. 8: MACH NUMBER CONTOUR PLOTS AT THE STATOR EXIT.

The leakage flow between stator and rotor was reported to be less than 0.6% (Denos et al. 1999). The resulting decrease in axial velocity would not be strong enough to explain the difference in incidence. A variation of the inlet total temperature within the frame of the reported test to test variation of 5% had no significant impact on the pressure prediction.

It can be seen in Fig. 7, that compared to the results with the rounded stator trailing edge configuration the ejection slot configuration gives a static pressure distribution, which is up to 2.1% higher on the pressure side and up to 4.2% higher on the suction side. The computations show the same tendency as the measurements when coolant gas is ejected, that is the pressure rises slightly on the suction side of the blade. These observations can be explained by the impact that the stator trailing edge cut out has on the flow field. The ejection slot cut moves the stator throat upstream and increases the throat width with 2% compared to the rounded edge configuration. As the stator is choked, the mass flow is also increased. The computed mass flow is 10.53 kg/s for the ejection slot configuration, which is 1.9% higher than for the rounded geometry. Coolant injection increases the mass flow by 1%, additionally. The mass flow, trailing edge geometry and coolant ejection has impact on the appearance of the stator trailing edge shock, as illustrated in Fig. 8. All together this leads to a static pressure rise of 2.6% behind the stator trailing edge for the ejection slot geometry compared to the rounded edge geometry (see also Table 1).

UNSTEADY COMPUTATIONS

Unsteady computations were performed with the rounded stator trailing edge configuration and with the ejection slot geometry with 3% coolant ejection. Both configurations show the same tendency when looking at the predicted time averaged static pressure distribution around the rotor blade at midspan. Compared with the steady computations the pressure rises up to 1.7% on the pressure side and up to 6% on the suction side of the rotor blade. See Fig. 9a and b. The discrepancy between the measurements and the computations remains unexplained, in fact the agreement between computations and measurements is better for the steady computations than for the unsteady computations. It is believed that the difference between the steady and unsteady computations is due to the inherent entropy rise over the mixing plane interface and higher order unsteadiness in the unsteady computations.

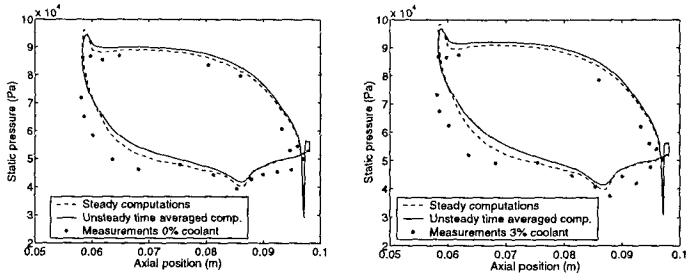

FIG. 9: STATIC PRESSURE DISTRIBUTION AROUND ROTOR BLADE AT MIDSPAN. 8a AND b CORRESPOND TO THE ROUNDED AND THE EJECTION SLOT GEOMETRY.

Fig. 10 and Fig. 11 compare measured unsteady pressure traces at 22 locations on the rotor suction and pressure surface at midspan with the computed unsteady results at the same locations.

Copyright © 2000 by ASME
Downloaded From: http://proceedings.asmedigitalcollection.asme.org/ on 02/03/2016 Terms of Use: http://www.asme.org/about-asme/terms-of-use

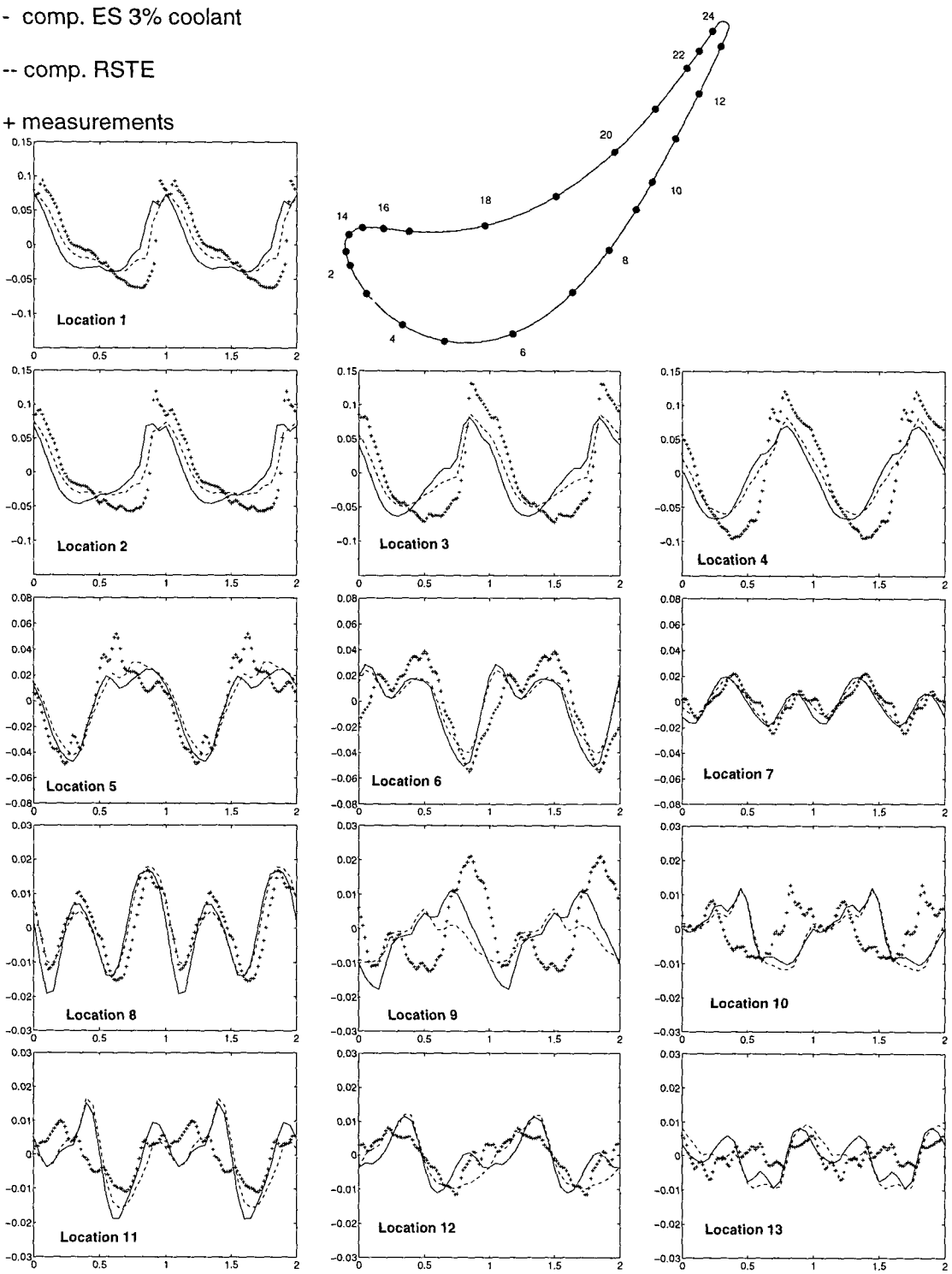

FIG. 10: MEASURED AND COMPUTED UNSTEADY PRESSURE TRACES ON THE ROTOR BLADE SUCTION SIDE AT MIDSPAN. DETAILS ARE VISUALIZED USING DIFFERENT Y-AXIS SCALING FOR THE FIGURE ROWS.

Copyright © 2000 by ASME
Downloaded From: http://proceedings.asmedigitalcollection.asme.org/ on 02/03/2016 Terms of Use: http://www.asme.org/about-asme/terms-of-use

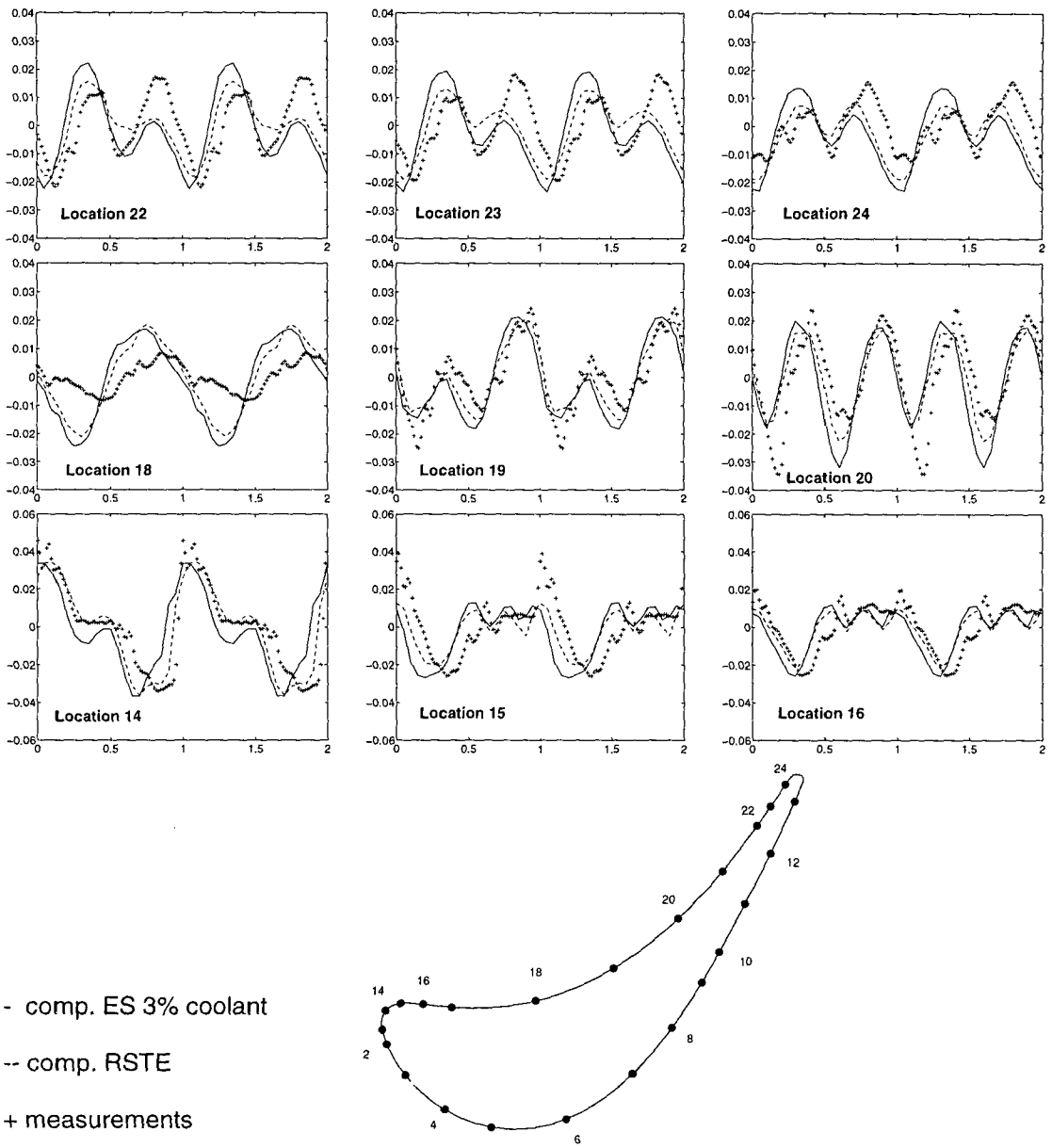

FIG. 11: MEASURED AND COMPUTED UNSTEADY PRESSURE TRACES ON THE ROTOR BLADE PRESSURE SIDE AT MIDSPAN. DETAILS ARE VISUALIZED USING DIFFERENT Y-AXIS SCALING FOR THE FIGURE ROWS.

The pressure traces are presented as perturbations from the time mean level $(P-P_{time\text{-}mean})/P_{01}$ over two pitches. To visualize details of the time dependent signal at all locations, the figures' y-axis scaling is changed from figure row to figure row so that all signals appear in about the same size. The measured pressure corresponds to the configuration with 3% coolant flow injection. Computation results are presented for both the rounded stator trailing edge geometry and the ejection slot configuration with 3% coolant ejection. The phase φ defines the position of the rotor blade with respect to the stator. Phase $\varphi = 0$ defines the position where the rotor and stator leading edges at blade midspan are axially aligned. $\Delta\varphi = 1$ corresponds to an angular rotor blade displacement of one stator pitch. The measured pressure traces are the result of a phase-locked averaging technique, which included measurements over three full rotor revolutions (129 periods). Method details are explained by Denos et al (1999). The presented computed pressure traces are the results for one computed period after convergence was reached. To give a better picture of the periodic behavior the data sets were doubled and presented over two periods.

Generally, the computations with the ejection slot geometry show good agreement in amplitude, phase and

Copyright © 2000 by ASME
Downloaded From: http://proceedings.asmedigitalcollection.asme.org/ on 02/03/2016 Terms of Use: http://www.asme.org/about-asme/terms-of-use

waveform with the measurements on the pressure side and half chord of the rotor blade's suction side. The steep periodic pressure rise on the front suction side of the rotor blade visible in pressure gauges 1-5 in Fig. 10 and gauge 14 in Fig. 11 originates from a weak stator trailing edge shock that impinges on the rotor blade surface and sweeps the suction side to the leading edge. The computations show good agreement in waveform and phase, but the amplitude is underestimated and the pressure rise is steeper in the measurements than in the computations. The latter may be attributed to the numerical smearing of the stator trailing edge shock. Denos et al. (1999) suggested that the double peak in the pressure fluctuations at the front suction side of the rotor blade could be attributed to the appearance of a separation bubble. In our computations the double peak is only observed for the ejection slot configuration, not for the rounded trailing edge configuration. A separation bubble was not observed. This would suggest that this double peak is a unique flow feature for the ejection slot configuration connected with the stator trailing edge shock pattern.

In the region of the pressure gauges 7 and 8 in Fig. 10 on the rotor suction side and gauges 20 to 24 in Fig. 11 on the pressure side a fluctuation with the double stator blade-passing period is observed. An explanation would be the alternating influence of the trailing edge shock and the stator wake in this part of the blade passage. The computations show good agreement with the measurements regarding the phase and the waveform, but differs in amplitude in gauges 20 to 24 in Fig. 11 on the pressure side of the blade.

Pressure gauges 9 to 13 in Fig. 10 on the suction side of the rotor blade are located downstream of a weak shock that stretches from the rotor suction side to the rotor trailing edge. The measured fluctuations show low amplitude, which is also captured by the computations. There is though a discrepancy between measurements and computations regarding both waveform and phase. This may be explained with the relatively stronger influence of random motion in this region.

The relatively strength of the flow features described above is visualized in Fig. 12 and Fig. 13. Fig. 12 shows the pressure traces at gauge 1 and 13 on the suction side and gauges 14 and 24 on the pressure side of the rotor blade with the same y-axis scaling. Fig. 13 shows RMS contour plots in the rotor blade passage at midspan. It can be seen that the direct influence of the stator trailing edge is restricted to a region, which stretches from the crown of the blade to the leading edge. This region shows significantly higher fluctuation amplitudes then the rest of the passage.

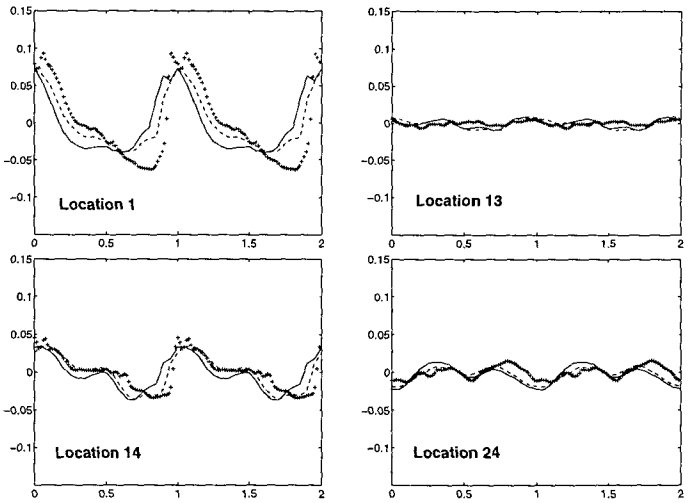

FIG. 12: MEASURED AND COMPUTED PRESSURE TRACES WITH THE SAME Y-AXIS SCALING.

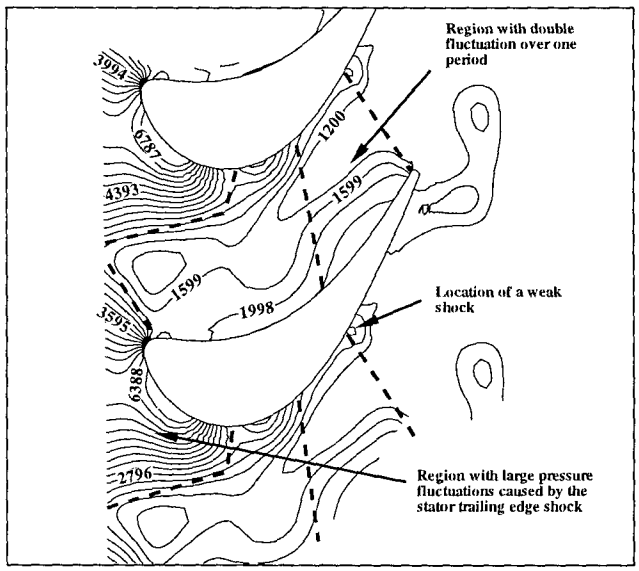

FIG. 13: STATIC PRESSURE FLUCTUATION RMS CONTOUR PLOT OF THE ROTOR BLADE PASSAGE AT MIDSPAN.

The unsteady flow features in the inter-blade region are shown in Fig. 14. The first column shows contour plots of the shock function $\frac{\mathbf{V}\cdot\nabla P}{a|\nabla P|}$ in the stator frame of reference for four time steps with $\Delta\varphi = 0.25$. The rotor blades are fixed and

Copyright © 2000 by ASME
Downloaded From: http://proceedings.asmedigitalcollection.asme.org/ on 02/03/2016 Terms of Use: http://www.asme.org/about-asme/terms-of-use

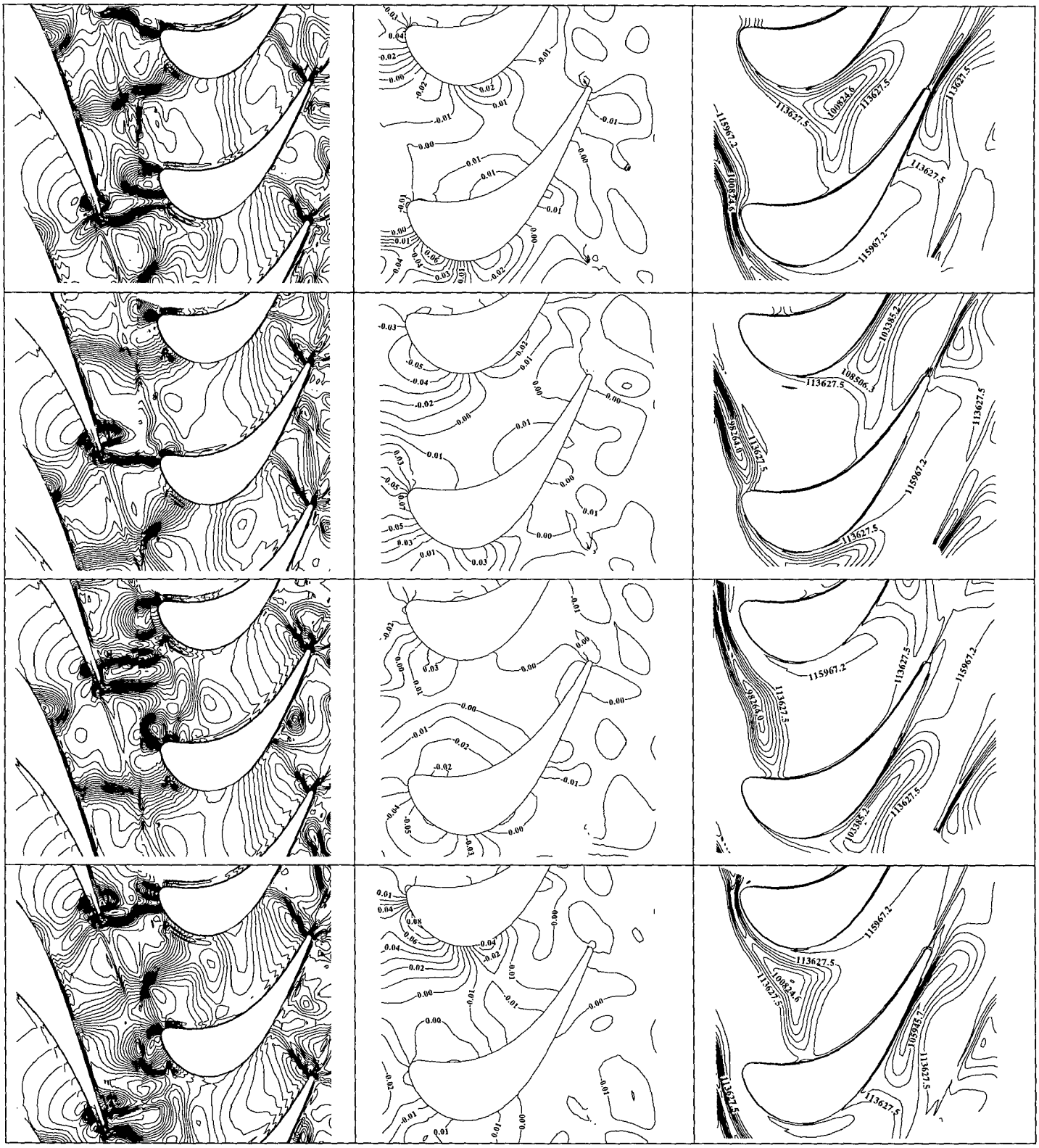

FIG. 14: SHOCK FUNCTION, STATIC PRESSURE PERTUBATION AND ENTROPY CONTOURS FOR FOUR CONSECUTIVE TIME STEPS.

Copyright © 2000 by ASME
Downloaded From: http://proceedings.asmedigitalcollection.asme.org/ on 02/03/2016 Terms of Use: http://www.asme.org/about-asme/terms-of-use

the stator blades move upwards in the picture series. The discontinuity at the sliding interface is due to post processing of the interface. Still, the shock can be traced from the stator trailing edge. The second and third column shows the static pressure perturbation field and the entropy field, visualizing the stator wake chopping.

In the first row the stator trailing edge shock impinges on the suction side of the lower rotor blade and in the second row the shock has moved to the leading edge of the blade. Downstream the shock the region of maximum positive pressure perturbation is located. The trailing edge shock has departed from the lower rotor blade in the third row, but it does not directly impinge on the suction side of the upper blade, instead it seems to interact with the stator trailing edge wake. The figures do not reveal any reflection of the trailing edge shock on the rotor suction surface, as was suggested by Giles (1988). This may be explained by the relative weakness of the shock and its interaction with the stator wake.

CONCLUSIONS

An investigation of the Brite Euram transonic turbine stage aerodynamics has been conducted with 3D steady and unsteady Navier-Stokes computations. The computations were performed with the nominal stator trailing edge geometry with ejection slots. Additionally, a simplified stator geometry with a rounded trailing edge was used.

Compared with measurements, both steady and unsteady computations showed a higher static pressure on the suction side of the rotor blade at midspan. The use of the Low Reynolds model instead of wall functions and a variation of the boundary conditions in the frame of the test to test variations had no significant effect on the results.

The rounded stator trailing edge configuration has a 2% smaller stator throat width compared with the ejection slot configuration. As the stator is choked, the computations gave a 1.9% lower mass flow for the rounded edge configuration. This explains the observed difference between the configurations regarding the static pressure distribution around the rotor blade.

The agreement between measured and computed unsteady static pressure perturbations is good on the pressure side and half chord of the rotor blade's suction side. Measurements and computations showed less good agreement downstream a weak shock on the suction side of the rotor blade.

The computations confirmed the experimental observation that the dominant influence of the stator trailing edge shock is restricted to a region, which stretches from the crown of the rotor blade along the front suction side to the rotor leading edge. Because of the relative weakness of the stator trailing edge shock and its interaction with the stator wake, a shock reflection on the rotor suction side was not observed in the computations.

The double peak in the leading edge region was not observed in the results from the computations with the rounded edge configuration. It was concluded that the pressure double peak was a unique flow feature for the ejection slot configuration, connected with the stator trailing edge shock pattern.

Altogether, the VOLSOL flow solver proved to be a useful tool for the prediction and interpretation of the unsteady flow field in the transonic turbine stage.

ACKNOWLEDGMENTS

This research was carried out under contract of the CEC as part of the BRITE EURAM Project "Turbulence modeling for unsteady flows in axial turbine stages". The authors wish to acknowledge this financial support as well as the support from KTH - the Royal Institute of Technology and Volvo Aero Corporation.

REFERENCES

Dahlander, P., Abrahamsson, H., Mårtensson, H., Håll, U., 1998, "Numerical simulation of a film cooled nozzle guide vane using an injection model", ASME paper 98-GT-439

Denos, R., Sieverding, C. H., Arts, T., Brouckaert, J. F., Paniagua, G. and Michelassi, V., 1999, "Experimental investigation of the unsteady rotor aerodynamics of a transonic turbine stage", IMECH *Conference Transactions, 3. European Conference on Turbomachinery*, pp. 271-287

Doorly, D. J. and Oldfield, M. L. G., 1985, "Simulation of the effects of shock wave passing on a turbine rotor blade", ASME *Journal of Engineering for Gas Turbines and Power*, Vol. 107, pp. 998-1006

Eriksson, L.-E., 1990 "A third order accurate upwind-biased finite volume scheme for unsteady compressible flow", VFA Report 9370-154, Volvo Aero Corporation, Trollhättan, Sweden

Giles, M. B., 1988, "Calculation of unsteady wake rotor interaction", AIAA *Journal of Propulsion and Power*, Vol. 4, pp. 356-362

Hilditch, M. A., Smith, G.S. and Singh, U. K., 1998, "Unsteady flow in a single stage turbine", ASME paper 98-GT-531

Michelassi, V., Martelli, F., Denos, R., Arts, T., Sieverding, C.H., 1998, "Unsteady heat transfer in stator-rotor interaction by two equation turbulence model", ASME paper 98-GT-243

Moss, R. W., Ainsworth, R. W., Sheldrake, C. D. and Miller, R. 1997, "The unsteady pressure field over a turbine blade surface: visualization and interpretation of experimental data", ASME paper 97-GT-474

Saxer, A. P., Giles, M. B., 1994, "Predictions of three-dimensional steady and unsteady inviscid transonic stator/rotor interaction with inlet radial temperature nonuniformity", ASME *Journal of Turbomachinery*, Vol. 116, pp. 347-357

Sieverding, C.H., Arts, T., Denos, R., Martelli, F.,1996, "Investigation of the flow field downstream of a turbine trailing edge cooled nozzle guide vane", ASME *Journal of Turbomachinery*, Vol. 118, pp 291-300

Copyright © 2000 by ASME

Downloaded From: http://proceedings.asmedigitalcollection.asme.org/ on 02/03/2016 Terms of Use: http://www.asme.org/about-asme/terms-of-use